PAPER • OPEN ACCESS

All-acoustic signal modulation and logic operation via defect induced cavity effects in phononic crystal coupled-resonator acoustic waveguides

New Journal of Physics
The open access journal at the forefront of physics

Deutsche Physikalische Gesellschaft DPG
IOP Institute of Physics

Published in partnership with: Deutsche Physikalische Gesellschaft and the Institute of Physics

OPEN ACCESS

RECEIVED
20 June 2019

REVISED
26 September 2019

ACCEPTED FOR PUBLICATION
18 October 2019

PUBLISHED
6 November 2019

PAPER

All-acoustic signal modulation and logic operation via defect induced cavity effects in phononic crystal coupled-resonator acoustic waveguides

Delfino Reyes[1,2], Ezekiel Walker[3], Yurii Zubov[2], Hyeonu Heo[2], Arkadii Krokhin[2] and Arup Neogi[2,4]

[1] Faculty of Science, Campus 'El Cerrillo', Autonomous University of the State of Mexico, Toluca, State of Mexico, Mexico
[2] University of North Texas, Department of Physics, Denton, TX, United States of America
[3] Echonovus Inc., Denton, TX, United States of America
[4] Advanced Manufacturing and Materials Processing Institute, University of North Texas, Denton, TX 76207, United States of America

E-mail: arup@unt.edu

Keywords: ultrasonic switches, phononic crystal, ultrasonic demultiplexing, defect engineering, acoustic waveguide

Abstract

A coupled resonant acoustic waveguide (CRAW) in a phononic crystal (PnC) was engineered to manipulate the propagation of ultrasonic waves within a conventional phononic bandgap for wavelength division multiplexing. The PnC device included two, forked, distinct CRAW waveguide channels that exhibited strong frequency and mode selectivity. Each branch was composed of cavities of differing volumes, with each giving rise to deep and shallow 'impurity' states. These states were utilized to select frequency windows where transmission along the channels was suppressed distinctly for each channel. Though completely a linear system, the mode sensitivity of each CRAW waveguide channel produced apparent nonlinear power dependence along each branch. Nonlinearity in the system arises from the combination of the mode sensitivity of each CRAW channel and small variations in the shape of the incident wavefront as a function of input power. The all-acoustic effect was then leveraged to realize an ultrasonic, spatial signal modulator, and logic element operating at 398 and 450 kHz using input power.

Introduction

Phononic crystals (PnCs), or elastic bandgap materials, are periodic arrangements of scatterers with divergent elastic properties from an ambient medium [1, 2]. Control of the size, shape, elastic or mass density contrast, and arrangement of the scattering elements allows for the artificial control of the propagation of elastic or pressure waves. Waveguides, specifically, are achieved by breaking the symmetry of the PnC using individual defects or defect arrays. The result is the transmission of limited modes and frequencies that would otherwise be forbidden [3, 4]. These guided acoustic modes are analogous to guided optical modes in photonic crystals and discrete states in the bandgap of a semiconductor with linear defects [5]. Defect arrays can result in the formation of acoustic metamaterials that are homogenized artificial materials with unprecedented functionalities [4, 6]. Similar to electromagnetic wave propagation in photonic crystal structures, the propagation of acoustic modes influenced by these localized defect modes in phononic structures can be designed to realize sensors [7], filters and waveguides [8, 9], and acoustic logic elements [10, 11] in the ultrasonic frequency domain.

Defect arrays are usually of the line form, opening up multimodal guided waves inside the phononic bandgap [3, 12]. Interference between guided bands can arise, leading to special phenomena such as avoided crossings [13, 14], mini-band gaps [15], and local resonators with strong amplification [12]. Another mechanism for waveguiding is similar to the tight-binding model in solids and is based on the coupling between defect cavities in crystals. Coupled-resonator acoustic waveguides (CRAWs) are coupled defect cavities in a PnC. They are of particular interest due to in particular its dispersion relation can be controlled through cavity design [16].

Propagation in coupled-resonator optical waveguides (CROWs), the optical equivalent of CRAWs, has been often described using the tight-binding approximation for cavities [17], the transfer-matrix method [18], or the coupled-mode method [19]. Each is dependent on the model of the cavity supercell with periodic boundaries and the evanescent waves that leak through the barrier walls. Escalante *et al* [20] found the optical models to be inadequate for PnCs. However, mechanisms of the tight-binding approximation and phonon propagation in linear chains of atoms were incorporated to form a new technique with improved accuracy for the CRAW modes. Importantly, as compared with the isolated cavity mode, oscillations in the dispersion relation arise as functions of the coupling strength [20]. As with CROWs, CRAW coupling strength is strongly dependent on the number of periods separating resonator cavities.

Combinations of non-identical cavities along a coupled-resonator defect pathway give rise to waveguides that, in practice, may exhibit strong frequency and polarization dependence. An approximately planar, monochromatic wavefront is composed of Fourier components with marginally varying orientations of the wave vector. For defect waveguides with turns or bends, wavefronts that maintain minor variations normally neglected in practice may produce wildly different output due to the strong sensitivity of CRAW modes along each section. Later in this work, we experimentally explore the approximately planar wavefronts generated by standard, unfocused 'planar' ultrasound sources, and show how the dependence of their approximately planar wavefronts on input power is used to interact with highly sensitive, distinct defect channel modes.

Currently, ultrasonic logic elements, including acoustic switches, are based on modulation of acoustic throughput signals using nonlinear responses in the materials comprising a PnC [21, 22]. Cylindrical polyvinylchloride inclusions squarely dispersed in air were used to build Boolean logic gates, specifically, for NAND, XOR, and NOT functions. These logic gates were derived from the phenomenon of Bragg scattering of acoustic waves by a periodic array operating in the audible frequency range [10]. Li *et al* [23] demonstrated an acoustic switch to realize OR and AND logic elements by exploiting nonlinearity in granular chains. In other works, a solid–solid, two-dimensional PnC was proposed as an element logic gate based on phase control, operating in the ultrasound range [24]. These examples leverage nonlinearity to introduce frequency multiplexing or demultiplexing for mechanical waves, then apply output conditions for logic elements.

To the best of our knowledge, there are no reports of an all-acoustic logic device based on the input properties of the ultrasonic wave that can be manipulated due to the geometry of the medium. Here, we manipulate the defect levels in a forked CRAW by incorporating coupled cavities of different geometry to produce an all acoustic logic device. The device operates fully within the realm of linear acoustics. However, apparent nonlinear behavior arises due to small deformations in the incident wavefront combined with the high sensitivity of each channel to the mode composition of the incident wave. This apparent nonlinearity is used to create an all-acoustic technique for controlling the transmission of ultrasonic waves when each Fourier component is transmitted in the linear regime. An asymmetric CRAW structure has been modeled and fabricated for demultiplexing of ultrasonic waves propagating through cavity defect waveguides, and the results reported below.

Results

Figure 1(a) presents a schematic of the PnC structure used for the design of the ultrasonic demultiplexing module. It consists of a matrix of 20 $\times$ 20 cylindrical rods of stainless steel immersed in water. The diameter, d, of the cylindrical rod is 1.6 mm with a length of 100 mm. The lattice constant, a, is 2 mm, resulting in a filling fraction, $f = \pi d^2/(4a^2) = 0.50$. Figure 1(b) shows the schematic of the two different kinds of defect cavity arrangements used for the coupled-resonators of the waveguide channels. These defect cavities were realized by removing 2 $\times$ 2 (Model I) and 2 $\times$ 4 (Model II) rods with a barrier of two scatterer layers between any adjacent cavities to ensure sufficient coupling. The top view of the device at the bottom for figure 1(a) shows the channel comprised of Model II defects where two scatterers are removed along the direction of sound propagation and four along the perpendicular.

The experimental transmission setup is shown in figure 1(c), where an emitter and detector are placed at opposing ends of the CRAW device. Prior literature has focused on either defect waveguides coupled to an adjacent cavity, or identical cavities separated along a line defect path. Figures 1(d) and (e) are the modeled and actual device. Here, the input is a CRAW based on Model I that is then forked into two defect waveguide branches comprised of Models I and II cavities. For clarity, 'G1' refers to the output channel of Model I based coupled-resonators, and 'G2' refers to the output channel of Model II resonators. The interplay between the relative signal output of G1 and G2 is utilized for both analysis of the mode sensitivity and selectivity, and the eventual all acoustic signal processing.

The bandstructure of the crystal with and without defects is given in figure 2. The bandstructure of each model was calculated using COMSOL Multiphysics. The linearized Navièr–Stokes coupled to Solid Mechanics

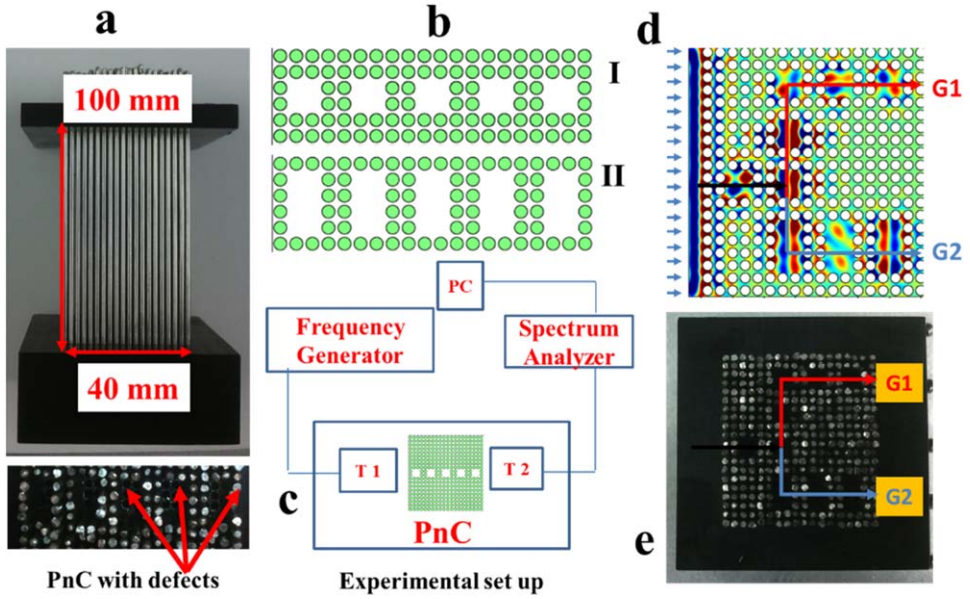

Figure 1. (a) Optical picture of the phononic crystal (PnC) (above) and its corresponding defect line (below). (b) Sketches of the coupled-resonator defect cavities (Models I and II). (c) Experimental set up used for measuring transmission spectra. (d) Field of propagating sound in the two channels (G1, G2) of the coupled resonant acoustic waveguide (CRAW) using COMSOL with its corresponding optical images in (e).

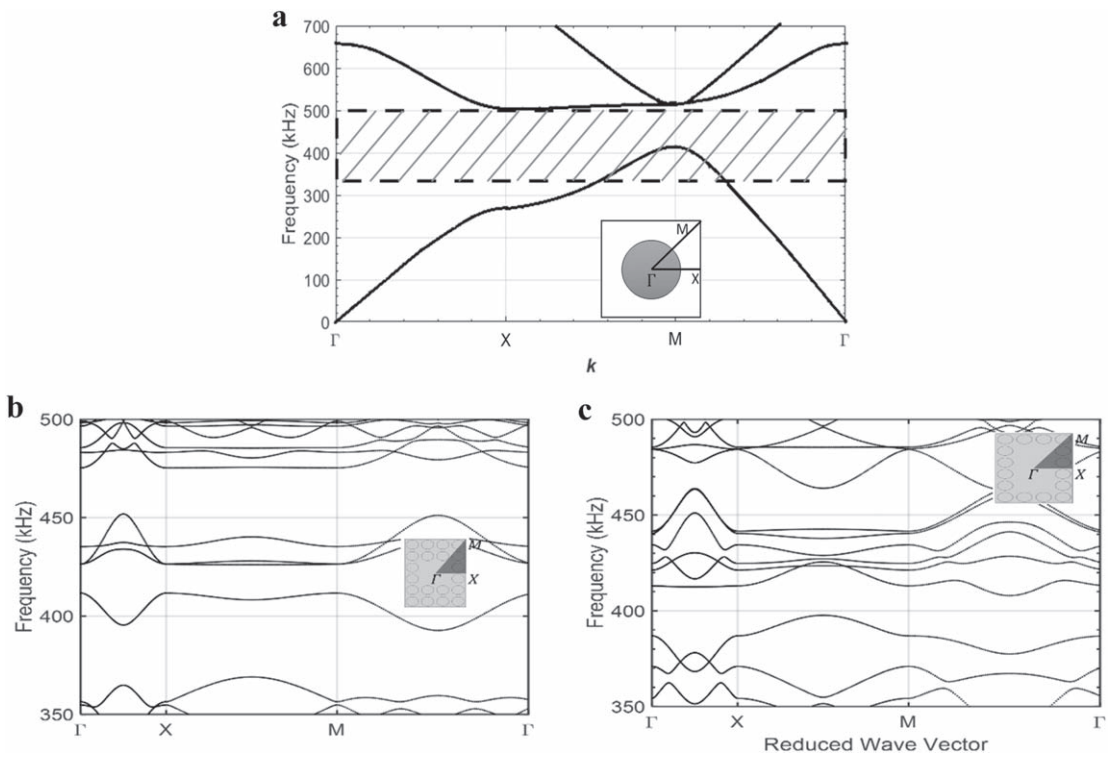

Figure 2. (a) Band diagram of the lattice of the CRAW device without defects. The structure is examined from 350 to 500 kHz indicated by dashed square. Inside the gap, the band diagram is given for a Model I (b) and Model II (c) defect using the superlattice approach. The defects open up different allowed modes as shown by their bandstructures.

physics engines and eigenfrequency solver were used with the superlattice approach to calculated the bandstructure along the irreducible Brillouin zone (IBZ) in each case. Figure 2(a) shows the first complete gap of the defect-free PnC from ~403–500 kHz. Inside these gaps, propagating modes arise when the Models I and II defects are introduced (figures 2(b) and (c)). As expected, the locations of the modes are distinct in some frequency ranges, and show overlap in others.

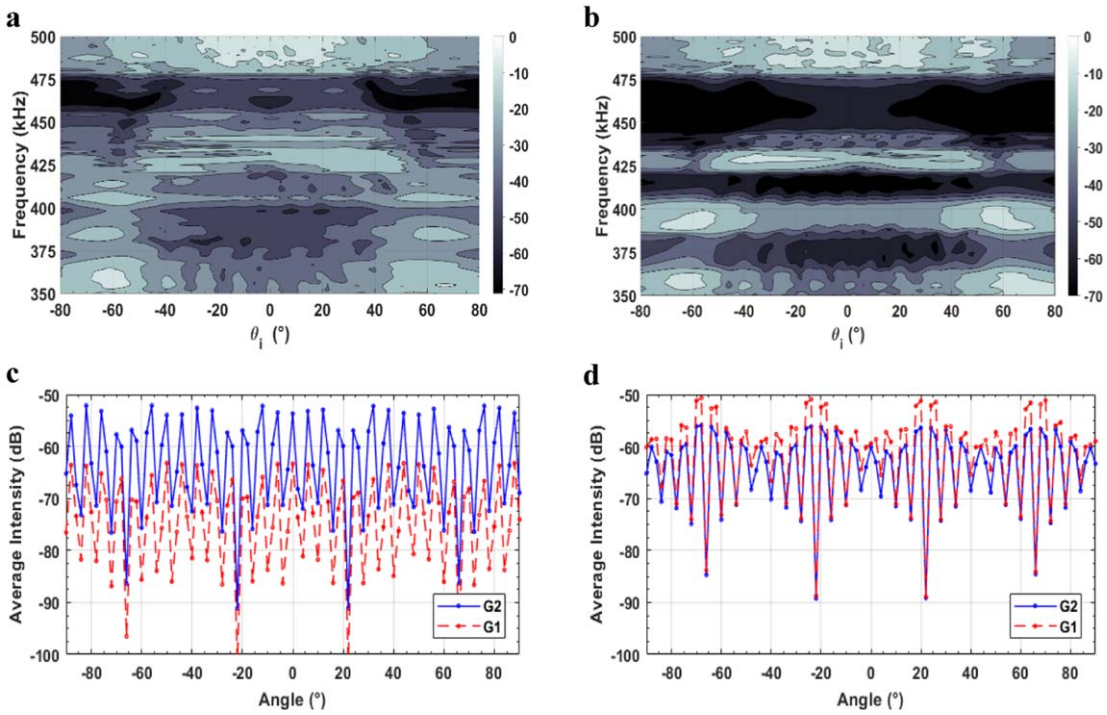

Figure 3. The numerically determined quasi-density of states for the upper G1 (a) and lower (b) channel G2 of the forked CRAW device. Transmission intensity was measured at the output for each channel for incident angles ranging from +90° to −90° with darker shading corresponding to decreased transmission. The defect modes of 450 (c) and 398 kHz (d) express varying mode coupling strength between channels.

The superlattice approach gives an indication of the additional propagating modes that will arise. However, this approach does not show a complete picture as scanning the IBZ only accounts for three propagation directions and approximates an *infinite* lattice. The CRAW device is comprised of two distinct cavities that are not periodically distributed through the entire structure. The asymmetry, the number of cavities in the defect channels, and potential for coupling between the channels is not accounted for in the superlattice approximation.

To more completely understand coupling, especially as it pertains to allowed modes as a function of wave vector, density of states provides additional, critical information. An increased density of states usually accompanies greater transmission. To approximate a more representative bandstructure for the device, the relative density of states as indicated by the transmission was evaluated using numerical techniques. A lack of a true reduced Brillouin zone resulted in the examination of wave propagation from incident angles of −90° to +90°.

COMSOL Multiphysics was used to numerically examine the frequency dependent propagation of sound through the CRAW device. The acoustics-solid interaction model was utilized in a 2D model with a frequency sweep using a plane wave radiation source. The scatterers were AISI 4130 Steel in water at 20 °C. Transmission through the CRAW branches G1 and G2 was measured by averaging the sound pressure level (SPL) at the output of each branch. For G1, the SPL was averaged in an area equal to the Model I defect cavity, and in an area equal to the Model II defect cavity at G2.

The angle and frequency dependent intensity contour map of figures 3(a) and (b) is indicative of the relative density of states of each channel. Darker shades correspond to lower intensity or lower density of states where sound propagation may be considered to be forbidden. As the intensity of the impinging wave is ideal in intensity, the dependence on angle can be used to extrapolate mode sensitivity. We especially focused on the region of 350–500 kHz.

The forked channels display significant variation in their dispersive, wave vector dependent transmission intensity as shown in figures 3(a) and (b) for G1 and G2 channels, respectively. The mode sensitivity for a specific direction of the wavenumber can qualitatively be compared by the rate the density of states changes with angle (figures 3(c), (d)). This is readily interpreted as each CRAW channel not only possessing different propagation modes, but also different variation in the sensitivity of the allowed modes.

To study the evolution of transport properties in relation to the number of defect cavities, 1, 3, and 5 cavities of Models I and II were placed in a straight line in the 20 × 20 PnC as illustrated in figure 1(c). The transmission was numerically examined using COMSOL (figure 4(a)) and experimentally measured for a sample with 5 defect

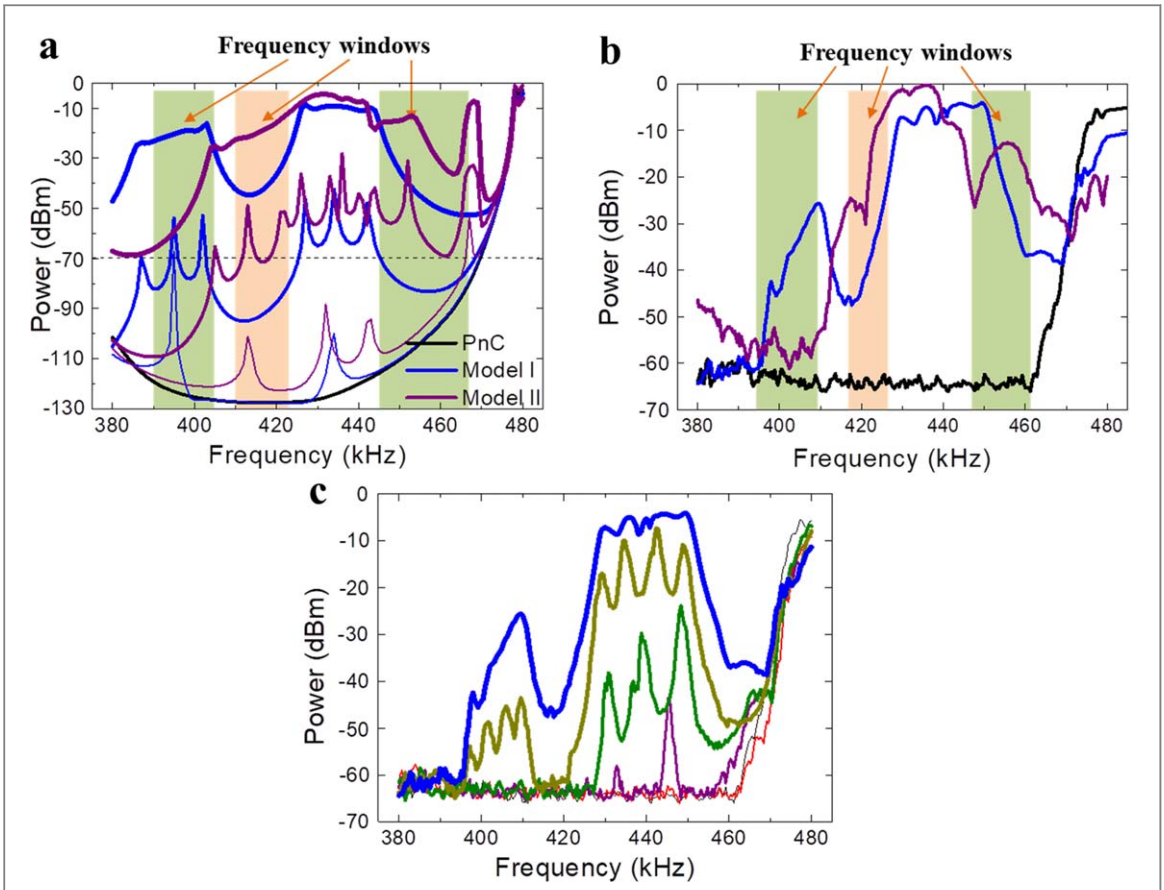

Figure 4. Transmission spectra through the PnC both with (non-black) and without (black) defects. (a) Spectra of PnC with 1, 3, and 5 2 × 2 (Model I, blue) and 2 × 4 (Model II, purple) generated numerically. The number of resonant peaks and overall transmission in the stopgap impurity states increases with number of defect cavities. (b) Experimental spectra of a PnC with 5 Model I (blue) and defects along the center of the crystal. Frequency windows denote where transmission is relatively suppressed along paths Model I/II while simultaneously allowed along Model II/I paths. (c) The resonances of the impurity states for 1–5 Model I defects are clearly demonstrated experimentally. Here, red-1 cavity, purple-2 cavities, green-3 cavities, yellow-4 cavities, blue-5 cavities. Splitting of the resonances occurs with increased cavities.

cavities (figures 4(b), (c)). Transmission is taken for a plane wave of 0° incidence, and compared to the crystal without defect waveguides.

The transmission for the defect-free crystal is indicated by the black lines in each graph of figure 4. The blue lines represent the crystal with Model I cavities, and purple for the Model II cavities in the same figure. Without G1 and G2, the defect-free PnC maintains a bandgap from 380 to 480 kHz. This stopband is examined more closely with the presence of Model I/II cavities due to defect states that arise in the transmission spectrum.

Similar to photonic or electronic structures, the presence of defect sites cause broken translational symmetry of the crystal and results in the transmission of usually forbidden, impurity states [5]. With a single Model I (2 × 2) defect at the center of the PnC, two shallow impurity states arise in the stopband at 393 and 494 kHz from the symmetric and antisymmetric modes (figure 3(a), blue line). As the number of cavities is increased, the mode degeneracy is split due to coupling between modes similar to what previous reports [8, 19]. Increasing Model I defects from 1 to 3 to 5 sequentially spaced cavities cause each mode to split to 3 then 5 resonances, as shown in figure 4(a) as blue lines. The defect waveguide, comprised of 5 defect cavities, effectively produces an intragap transmission band of the same nature as an impurity zone in doped semiconductors (figures 4(a), (b), highest blue line). Similar behavior is found for the sequence of 1, 3, and 5 Model II (2 × 4) cavities. However, whereas the 2 × 2 cavity exhibits double degeneracy in this gap, the 2 × 4 causes deeper impurity states to arise with four associated base defect states (figure 4(a), purple lines). The increase to 5 sequential periods and subsequent splitting of the symmetric and antisymmetric modes due to coupling between cavities eventually results in two, distinctly different impurity zones for both the Model I and Model II defect waveguides (figures 4(a), (b) highest blue and purple lines). Both numerical and experimental results confirm the appearance of cavity modes and the subsequent splitting in mode degeneracy with increasing number of cavities (figures 4(b), (c)).

It has been demonstrated that depending on the geometry of the defects, waves at two discrete frequencies are selectively guided along the two distinct pathways due to the dependence of coupling strength on

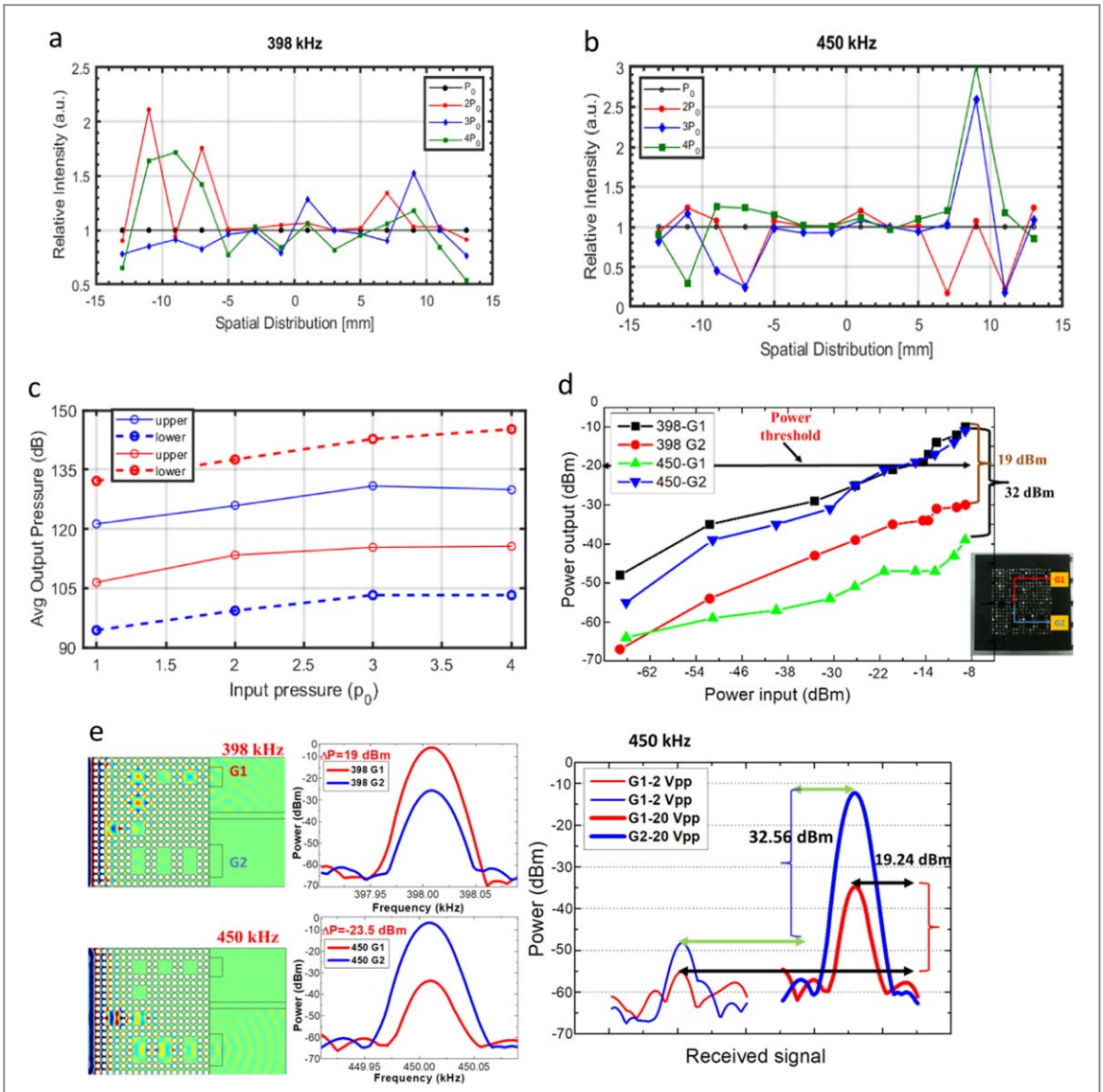

Figure 5. Impact of the incident wavefront profile on output through G1 and G2 as a function of input power. Relative, normalized spatial intensity profile for (a) 398 and (c) 450 kHz. Increasing power leads to nonlinear ratio between G1 and G2 as shown numerically (c) and experimentally (d). (e) 398 kHz more strongly couples to the G1 channel while 450 kHz couples more strongly to G2 as shown by the pressure fields (left, middle). For 450 kHz, the mode sensitivity combined with increase from 2 *V*pp to 20 *V*pp leads to nearly 13 dB increase in transmission in G2 compared with G1.

wavenumber [3, 16, 20]. As the number of defect cavities surpasses four, the mode degeneracy splits sufficiently to effectively create intragap transmission bands shown by the highest transmission lines in figure 3. Frequency windows around 398, 418, and 450 kHz were selected based on the confluence of transmission along the G1 channel versus suppression along the G2 channel and vice versa. Selected regions are indicated in figures 3(a) and (b) by colored bars. Green bars indicate where transmission is higher along channel G1, composed of Model I cavities, and orange indicative of preferential transmission along the G2 channel of Model II cavities. The mode selectivity of the CRAW defect pathways is thus demonstrated by the presence of forbidden transmission for one channel while allowed transmission for the other.

The coupling strength is dependent on the incident angle of a wavefront and frequency (figure 3). For the experiment, the 25 mm Panametrics V301 0.5 MHz unfocused plane wave transducer was found to have a spatial wavefront pressure gradient that was dependent on power (figures 5(a), (b)). The relative spatial intensity compares the spatial intensity of four different input powers where each spatial intensity is normalized to its maximum at the incident plane of the PnC. Variation in the relative spatial intensity thus shows variation in the shape of the incident wavefront and mode composition as a function of input power. It should be noted that though the radius of the active element of the emitter is 12.5 mm, 5 mm, or 16% of the active element area, maintains consistently low variation in relative intensity.

The slight variations in the wavefront, however, produce effectively nonlinear behavior through the system which contains only linear elements. Note, that nonlinear behavior caused by geometrical factors in a pure linear

regime is known for several mechanical systems [25, 26]. Here, focus is given to the frequencies of 398 and 450 kHz. Both reside in the frequency windows where transmission is strong along one channel and suppressed in the other. The experimentally measured wavefront shape was incorporated into the incident wave for the numerical model, and the output intensity at each port recorded (figure 5(c)). Additionally, the input power into the transducer was varied without perturbing the setup, and the transmission intensity at each port recorded (figure 5(d)). For both numerical and experimental results, comparison of the shape and slopes of the input versus output lines for 398 and 450 kHz in figures 5(c) and (d) indicates the relative transmission efficiency between G1 and G2. Linear response is indicated by a constant ratio of the input versus output between G1 and G2. However, the variation in shape and slope between G1 and G2 in figures 5(c) and (d) for both the experimental and numerical results indicate variation in the input versus output ratio.

In agreement with the selected frequency windows, 398 kHz enjoys strongly preferential propagation along G1 with suppression along G2 (figure 5(e)). At 450 kHz, the opposite occurs, as propagation along G2 is supported and suppressed along G1. This trend maintains regardless of input power (figures 5(c) and (d)). However, the high mode sensitivity of G1 and G2 produce apparent nonlinear power dependence due to the slight variations in the wavefront in the experimental measurements due to changing input power. The phenomenon happens despite all the elements of the system operating in the linear regime. For example, when input power into the system increases ~100×, the output for 450 kHz increases nearly 100× for G2, but only 10× for G1.

Discussion

The output intensity shows a strong nonlinear dependence on the shape of the wavefront profile. The wavefront shape from the V301 transducer shows power dependence, and can thus produce nonlinear output through each CRAW branch by varying the input power to the emitter. This effect is utilized to modulate the output between G1 and G2 and create a logic device of purely mechanical waves. The logic device in this work focuses on the high mode sensitivity of G1 and G2 combined with the selection of the 'frequency windows' identified in figures 4(a) and (b).

The three frequency windows, approximately located between 388–405 kHz, 412–422 kHz and 445–455 kHz, exhibit high intensity propagation along one channel with corresponding low intensity in the other. Discussion is limited to 398 and 450 kHz as they maintain the desired behavior of preferred propagation along G1 for 398 kHz and G2 for 450 kHz. As there are two defect pathway channels, propagation along one channel indicates an independent supported CRAW mode. The strong transmission and suppression results in a power differential between G1 and G2 reaching in excess of 100×. Based on the experimental equipment and arrangement, a 100× increase in power results in a 4× increase in pressure.

Comparison of the power differential at the ports G1 and G2 in the frequency windows demonstrates spatial modulation of the energy output. Depending on input frequency, one can control not only the spatial location at which the acoustic energy is transmitted with higher power, but also the differential between the two ports. Figure 5(e) illustrates frequency-based spatial modulation. The selection of 450 kHz will direct energy to G2 while selection of 398 kHz will direct to G1.

Splitting does not occur for all frequencies. Figure 1(d) is the sound propagation field for 434 kHz. 434 kHz resides well within the stopgap with propagation confined to the defect waveguide. However, unlike 398 kHz and 450 kHz, transmission is strongly supported along both channels. Experimental results support the general trend in spatial energy modulation as G2 experiences differentials of +23.5 dB for 450 kHz, while a +19 dB differential at G1 at 398 kHz.

The sensitivity of coupling to the spatial distribution of the incident wavefront in the CRAW branches and the resultant output is demonstrated in figure 5. Both, bending and tunneling of waves in PnCs have been reported [3, 27], but little has been reported on the impact that split channels with different modes can have on signal output. For this work, the input power into the emitting transducer in the bistatic setup was varied from 2 to 20 V, and the amplitude of the output in the frequency windows recorded (figures 5(c), (d)). In a device with a linear response, the slope in the output for each channel should remain equal for a single frequency. However, the effects of increasing input power on the shape of the incident wavefront cause coupling in the CRAW branches that varies with input power.

The result is a nonlinear response demonstrated by an input to output power dependence that is not equal between G1 and G2. Essentially, the ratio, or efficiency, of input to output power is dependent on both the channel and frequency. Figure 5(e) illustrates this point as, for 450 kHz, output through G1 increases ~19 dBm from 2to 20 V input, while output through G2 increases ~32 dBm for the same differential in input power. This is due to the small experimental variation in the wavefront pressure gradient (figures 5(a), (b)) as dependent on input power, and the strong mode sensitivity on the output efficiency of G1 and G2.

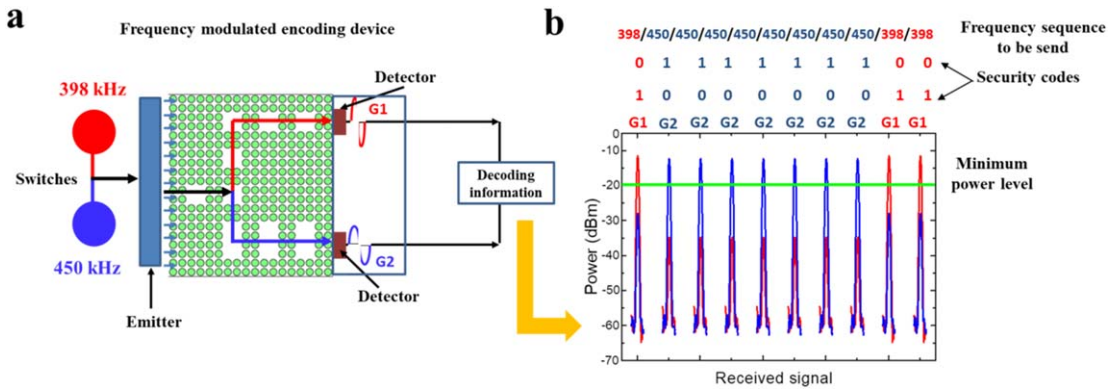

Figure 6. (a) Sketch of the acoustic logical device for encoding process with a broadband input pulse with the components of 398 and 450 kHz controlled with intent, (b) demultiplexing is accomplished by spatial modulation of the power output by varying the 398 or 450 kHz frequency components of the pulse. Modulation of the frequency components is achieved through pulse shaping.

Encoding with the device is accomplished as sketched in figure 6(a): a constant input power utilizes the observed differential power output between the power at ports G1 and G2 at 398 kHz and 450 kHz. The two frequencies were selected from the frequency windows in which effectively nonlinear power dependence was demonstrated as described earlier. Broadband, Fourier transformed pulses that included 398 kHz and 450 kHz components were used. A threshold of −20 dBm was set and combined with the condition if G1 exceeded G2, the binary output was '0', and '1' if G2 exceeded G1. The 398 and 450 kHz components of the pulse were adjusted so that for a '0', the 398 kHz component exceed the 450 kHz component, and vice versa to generate a '1'.

This demultiplexing process of broadband pulses by the defect engineered PnC device to discriminate selective frequency components is illustrated in figure 5(b). In figure 5(b), the binary code is (0111111100), resulting from the frequency inputs sequence (398/450/450/450/450/ 450/450/450/450/398/398), which corresponds to decimal number 508. Interestingly, if the interpretation is inverted i.e. with G1 as '1' and G2 as '0', the binary code becomes (100000011) and the encoding number 259.

The described possible process for encoding information is proposed as an innovative and simple way to use an acoustic metamaterial for information transmission and possible encryption based in the observed nonlinear response. Phononic and mechanical waves may not provide information transmission speeds comparable with electronics due to higher possible transmission rates of electrons and electronic information. The proposal to use phononic structures for logic elements or acoustic signal treatment for logic operation has been reported [21–24]. However, the reported results here can enable one the possible design of novel acoustic devices not only for the selective transmission but also the spatial control of acoustic energy flow, which is not used in the cited references.

Conclusion

Experimentally increasing power into a single element ultrasound source causes minor wavefront variations that can be functionalized to produce apparent nonlinear effects in a linear CRAW system. The use of a forked CRAW where one fork is a coupled waveguide of shallow impurity states, and the other comprised of deep impurity states allows for spatial modulation of energy within select frequency ranges. Additionally, the high mode sensitivity of each fork allows for apparent nonlinear effects in a linear system by introducing minor variations in a planar, incident wavefront. Output signals at 398 or 450 kHz can be spatially deflected from one output port to another point of the output port of a phononic device by controlling the spatial pressure gradient of the incident broadband acoustic signal. In this work, this is accomplished due to small variations in the emitted pressure gradient as a function of input power without otherwise perturbing the system. The realization of an ultrasonic logic element has the potential applications for underwater communications. The simple technique of controlling the acoustic energy via the defects in the phononic metamaterial structure can be applied to filter, confine, or guide acoustic energy for underwater wireless communications and sensing.

In conclusion, defect engineered structures within a multifunctional PnC lattice have been utilized to control ultrasonic wave propagation for designing ultrasonic switches and demultiplexers. The structures have been designed using computational modeling and experimentally verified using ultrasonic spectroscopy. The propagation of the beam through the waveguide is induced by the defects in the PnC which results in tunneling through the defect states and interference due to the reflected waves at the bends. In the absence of the defects, as

these modes lie within the stopgap of the PnC, these cannot propagate through the periodic structure. The defect cavity within the PnC waveguide induces nonlinear power dependent behavior that can be utilized for amplitude modulation of the ultrasonic signal. This leads to signals at the output that can be controlled not only by selecting the frequency but also the power of the input signal. Both amplitude and frequency modulated logic operation has been demonstrated. A sequence of spatially resolved signals transmitted at a discrete frequency through these optimized structures demonstrate the functionality of phononic logic devices.

Experimental details

Transmission spectra of these phononic devices were experimentally recorded using ultrasonic spectroscopy. For figures 3(b) and (c), two immersion transducers (Olympus V301 0.5 MHz) were used as an emitter and a receiver (figure 1(c)). These were placed in a bistatic, thru-transmission setup, 44 mm apart, with the CRAW PnC structure in between, and transducer faces set 2 mm from the surface of the device. Ultrasonic waves in the 200–800 kHz range were generated from a Teledyne Lecroy, Wave Station-2012 function generator. The signal output from the phononic device was recorded using a Tektronix-MDO3024b spectrum analyzer. PnC and transducers were located in an acrylic tank filled with DI water at room temperature.

Data for figure 4 was measured using a thru-transmission setup with a 0.5 mm Müller-Platte MVA10 needle probe hydrophone coupled to an amplifier. The hydrophone was placed 2 mm away from G1/2 channel output. The local acoustic intensity at specific frequencies in ports G1 and G2 were measured with water at ambient room temperature (~21.0 °C) and the results plotted.

Acknowledgments

This work is supported by National Science Foundation sponsored EFRI: NewLAW project entitled, 'GOALI: EFRI NewLaw: Non-reciprocal effects and Anderson localization of acoustic and elastic waves in periodic structures with broken P-symmetry of the unit cell' Award #1741677. The support from UAEM and AMMPI Seed Grants are also acknowledged. DR also acknowledge to UAEM for the funds for short research stays at UNT..

ORCID iDs

Arup Neogi https://orcid.org/0000-0003-3075-8683

References

[1] Kushwaha M S 1996 Classical band structure of periodic elastic composites *Int. J. Mod. Phys.* **10** 977
[2] Haberman M and Guild M 2016 Acoustic metamaterials *Phys. Today* **69** 42–8
[3] Khelif A, Choujaa A, Benchabane S, Djafari-Rouhani B and Laude V 2004 Bending and branching of acoustics waves in two-dimensional phononic crystal waveguides *Appl. Phys. Lett.* **84** 4400–2
[4] Khelif A, Choujaa A, Djafari-Rouhani B, Wilm M, Ballandras S and Laude V 2003 Trapping and guiding of acoustic waves by defect modes in a full-band-gap ultrasonic crystal *Phys. Rev.* B **68** 214301
[5] Bulgakov E, Pichugin K and Sadreev A 2011 Symmetry breaking for transmission in a photonic waveguide coupled with two off-channel nonlinear defects *Phys. Rev.* B **83** 045109
[6] Ma G and Sheng P 2016 Acoustic metamaterials: from local resonances to broad horizons *Sci. Adv.* **2** e1501595
[7] Villa S, Betancur D, Torres R, Kyriacou P and Lucklum R 2017 Differential phononic crystal sensor: towards a temperature compensation mechanism for field applications development *Sensors* **17** 1960
[8] Lazcano Z, Meza O and Arriaga J 2014 Localization of acoustic modes in periodic porous silicon structures *Nanoscale Res. Lett.* **9** 419
[9] Oudich M, Badreddine M and Hou Z 2010 Propagation of acoustic waves and waveguiding in a two-dimensional locally resonant phononic crystal plate *Appl. Phys. Lett.* **97** 193503
[10] Bringuier S, Swinteck N, Vasseur J, Robillard J-F, Runge K, Muralidharan K and Deymier P 2011 Phase-controlling phononic crystals: realization of acoustic Boolean logic gates *J. Acost. Soc. Am.* **130** 1919
[11] Hatanaka D, Darras T, Mahboob I, Onomitsu K and Yamaguchi H 2017 Broadband reconfigurable logic gates in phonon waveguides *Sci. Rep.* **96** 12745
[12] Jiang W, Feng D, Xu D, Xiong B and Wang Y 2016 Experimental investigation of energy localization in line-defect resonator based on silicon locally resonant phononic crystal *Appl. Phys. Lett.* **109** 161102
[13] Wang Y-F, Maznev A and Laude V 2016 Formation of Bragg band gaps in anisotropic phononic crystals analyzed with the empty lattice model *Crystals* **6** 52
[14] Alonso-Redondo E, Schmitt M, Urbach Z, Hui C M, Sainidou R, Rembert P, Matyjaszewski K, Bockstaller M R and Fytas G 2015 A new class of tunable hypersonic phononic crystals based on polymer-tethered colloids *Nat. Commun.* **6**
[15] Romero-García V, Vasseur J O, Hladky-Hennion A C, Garcia-Raffi L M and Sánchez-Pérez J V 2011 Level repulsion and evanescent waves in sonic crystals *Phys. Rev.* B **84** 212302
[16] Sainidou R, Stefanou N and Modinos A 2006 Linear chain of weakly coupled defects in a three-dimensional phononic crystal: a model acoustic waveguide *Phys. Rev.* B **74** 172302

[17] Kaina N, Causier A, Bourlier Y, Fink M, Berthelot T and Lerosey G 2017 Slow waves in locally resonant metamaterials line defect waveguides *Sci. Rep.* **7** 15105
[18] Hussein M 2009 Reduced Bloch mode expansion for periodic media band structure calculations *Proc. R. Soc.* A **465** 2825–48
[19] Han W, Zhou J, Song H, Meng Y and Yang J 2015 Analysis of compound coupled-resonator optical waveguide by coupled-mode theory *Optik—Int. J. Light Electron Opt.* **126** 1114–6
[20] Escalante J M, Martinez A and Laude V 2013 Dispersion relation of coupled-resonator acoustic waveguides formed by defect cavities in a phononic crystal *J. Phys. D: Appl. Phys.* **46** 475301
[21] Ganesh R and Gonella S 2015 From modal mixing to tunable functional switches in nonlinear phononic crystals *Phys. Rev. Lett.* **114** 054302
[22] Bilal S, Foehr A and Daraio C 2017 Bistable metamaterial for switching and cascading elastic vibrations *Proc. Natl Acad. Soc.* **114** 4603–6
[23] Li F, Anzel P, Yang J, Kevrekidis P G and Daraio C 2014 Granular acoustic switches and logic elements *Nat. Commun.* **5** 5311
[24] Vasseur J, Morvan B, Tinel A, Swinteck N, Hladky-Hennion A-C and Deymier P 2012 Experimental evidence of zero-angle refraction and acoustic wave-phase control in a two-dimensional solid/solid phononic crystal *Phys. Rev.* B **86** 134305
[25] Hertz H 1882 Über die Berührung fester elastischer Körper *J. Rein. Angew. Math.* **92** 156–71
[26] Gusev V, Jiménez N and Sánchez-Morcillo V J 2019 Nonlinear waves in phononic rotational lattices *Book of abstracts of the 5th Int. Conf. on Phononic Crystals/Metamaterials, Phonon Transport & Topological Phononics* p 8
[27] Benchabane S, Gaiffe O, Salut R, Ulliac G, Laude V and Kokkonen K 2015 Guidance of surface waves in a micron-scale phononic crystal line-defect waveguide *Appl. Phys. Lett.* **106** 081903